IOPscience iopscience.iop.org

Home Search Collections Journals About Contact us My IOPscience

Magnetic properties of stoichiometric $NpFe_4Al_8$

This article has been downloaded from IOPscience. Please scroll down to see the full text article.

2005 J. Phys.: Condens. Matter 17 909

(http://iopscience.iop.org/0953-8984/17/6/010)

View the table of contents for this issue, or go to the journal homepage for more

Download details:
IP Address: 129.252.86.83
The article was downloaded on 27/05/2010 at 20:19

Please note that terms and conditions apply.

INSTITUTE OF PHYSICS PUBLISHING JOURNAL OF PHYSICS: CONDENSED MATTER

J. Phys.: Condens. Matter **17** (2005) 909–922 doi:10.1088/0953-8984/17/6/010

Magnetic properties of stoichiometric $NpFe_4Al_8$

A P Gonçalves[1], M Almeida[1], C Cardoso[2], T Gasche[2,3], M Godinho[2], P Boulet[4], E Colineau[4], F Wastin[4] and J Rebizant[4]

[1] Departamento de Química, Instituto Tecnológico e Nuclear/CFMCUL, P-2686-953 Sacavém, Portugal
[2] CFMCUL/Departamento de Física, FCUL, 1749-016 Campo Grande, Lisboa, Portugal
[3] CINAMIL/Laboratório de Física, Academia Militar, Lisboa, Portugal
[4] European Commission, JRC, Institute for Transuranium Elements, Postfach 2340, D-76125 Karlsruhe, Germany

Received 15 October 2004, in final form 4 January 2005
Published 28 January 2005
Online at stacks.iop.org/JPhysCM/17/909

Abstract

The compound $NpFe_4Al_8$ was prepared by direct arc melting of the constituent elements, followed by annealing. It crystallizes in the $ThMn_{12}$-type structure (space group $I4/mmm$, $a = 8.7480(5)$ Å, $c = 5.0372(4)$ Å), with the iron atoms completely and only occupying the 8f positions. Magnetization measurements ($T = 2$–300 K, $B = 0$–7 T) show a ferromagnetic-type transition at $T_C = 135(2)$ K and a second anomaly at 118(3) K. The low temperature magnetization cycle is characterized by a hysteresis with a step similar to that previously observed for UFe_4Al_8 single crystals. First-principles density functional theory calculations of the $NpFe_4Al_8$ band structure point to a magnetic structure similar to that of UFe_4Al_8, in agreement with the observed magnetization cycle. The calculations indicate that the neptunium moment is aligned along one of the a or b axes, and the iron moments form a noncollinear structure in the a–b plane, with the antiferromagnetic and ferromagnetic contributions perpendicular and antiparallel to the neptunium spin moment, respectively.

1. Introduction

The UFe_4Al_8 compound has been extensively studied during the last few years due to its physical properties [1–10]. It crystallizes in the tetragonal $ThMn_{12}$-type structure [11] with the iron atoms occupying the 8f positions. Unlike the case for RFe_4Al_8 (R = magnetic rare earth) compounds, where the orderings of the rare earth and iron magnetic moments develop at different temperatures [12], only one ferromagnetic-type transition temperature is observed for UFe_4Al_8 [6]. Single-crystal neutron experiments showed that this compound has a complex magnetic structure, with the uranium moments ferromagnetically aligned along the a or b axes and almost perpendicular to the iron moments, which lie in the a–b plane with a slightly canted antiferromagnetic structure [6]. This magnetic structure is associated with

an anomalous magnetization process, first detected via a giant-magnetoresistance anomaly, in which the magnetization remains blocked perpendicularly to the applied magnetic field during the magnetization cycle [7]. A Mössbauer study on a UFe_4Al_8 single crystal confirms this anomalous magnetization cycle with the perpendicular blocking of the ferromagnetic component as a metastable state [5]. Relativistic band structure calculations for UFe_4Al_8 agree with the experimentally determined magnetic structure and indicate that the uranium magnetism is induced by the antiferromagnetism of the iron sublattice [3].

The isostructural $NpFe_4Al_8$ compound has not been studied so far. The only previous work was carried out on a nonstoichiometric $NpFe_4Al_{6.4}$ sample, where high quality crystal structure refinement from powder neutron diffraction data indicates a 40% aluminium deficiency in the 8j position [13]. This nonstoichiometry was also reflected in the refined positional parameter for the 8j position, $x = 0.326(5)$, significantly different from the one expected for the ideal $ThMn_{12}$-type structure ($x \approx 0.28$). Mössbauer effect and neutron diffraction studies showed that the neptunium and iron moments order magnetically at close temperatures, 115(15) and 130(10) K, respectively. An antiferromagnetic ordering of the iron moments and a ferromagnetic ordering of the neptunium moments, both along the *c*-axis, were previously proposed for this sample [14]. The same sample (with the same cell and positional parameters) was later reported as having the $NpFe_4Al_8$ composition [14–16], but maintaining the proposed magnetic structure. Subsequent analysis of AC and DC susceptibility, neutron diffraction and Mössbauer studies led to the suggestion of a spin-glass state at low temperatures for this sample [15].

$AnFe_4Al_8$ can be seen as the only compound in the general series of $AnFe_xAl_{12-x}$ semiordered alloys and, as was well described for uranium, slight deviations from the ideal composition are expected to have dramatic effects on the magnetic properties [17]. In these compounds the coupling between the iron and f-element sublattices is expected to change from uranium to neptunium due to a higher localization of the neptunium 5f electrons. This can lead to significantly different magnetic properties of isostructural uranium and neptunium compounds. In this paper we present detailed structural analysis, from powder and single-crystal x-ray diffraction data, and magnetic characterization of a $NpFe_4Al_8$ polycrystalline sample. A theoretical analysis of the $NpFe_4Al_8$ magnetic structure is also presented and compared with the experimental data.

2. Experimental details

A polycrystalline sample with $NpFe_4Al_8$ nominal composition, weighing ∼1 g, was prepared by arc melting the metal constituents in a water-cooled copper crucible under a Zr-gettered high purity argon atmosphere. The starting elements were used as ingots, supplied by Merck (iron and aluminium) and by LANL (neptunium), with purity higher than 99.9%. Repeated melting was used in order to ensure a better homogeneity of the sample, the weight losses being less than 0.5 wt%. Part of the sample was wrapped in tantalum foil and annealed for 15 days at 600 °C under vacuum.

Samples for powder x-ray diffraction were prepared by mixing $NpFe_4Al_8$ (as-cast and annealed) with epoxy glue, in order to minimize radioactive contamination risks. Room temperature x-ray powder diffraction measurements were performed on a Bragg–Brentano Siemens D500 diffractometer up to $2\theta = 140°$, with a Cu Kα radiation, a step size of 0.02° in 2θ and an accumulation time of 2 s/step. The diffraction patterns were analysed by a Rietveld-type profile refinement method using the FULLPROF program [18] in order to determine the $NpFe_4Al_8$ cell parameters and check the purity of the samples.

Small single crystals suitable for x-ray measurements ($\sim 0.1 \times 0.1 \times 0.1$ mm^3) were isolated from the as-cast polycrystalline material and mounted on goniometer heads. X-ray

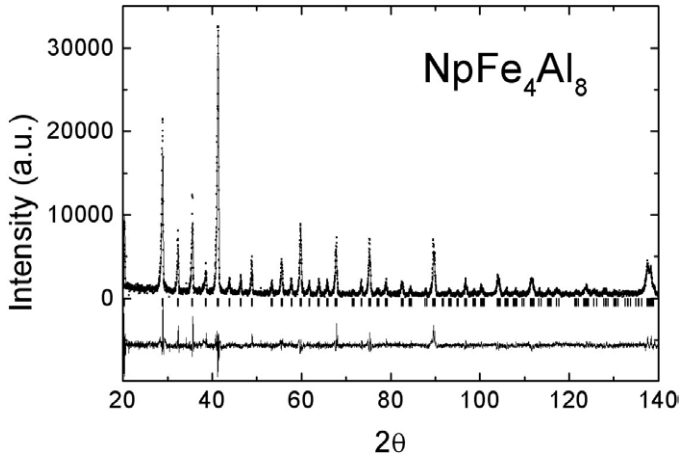

Figure 1. Observed (symbols) and calculated (curve) x-ray powder diffraction patterns for $NpFe_4Al_8$. The lower curve represents the difference between the observed and calculated profiles.

single-crystal diffraction data were collected using a four-circle diffractometer Enraf-Nonius CAD-4 with graphite monochromatized Mo Kα radiation ($\lambda = 0.709\,30$ Å). The data were recorded at room temperature in a ω–2θ scan mode ($\Delta\omega = 0.80 + 0.35\text{tg}\theta$). During the data collection, three reflections were monitored for intensity at 120 min intervals, and orientation control was carried out every 400 reflections; no variation in the intensity larger than 5% was observed. A total of 2238 reflections ($-12 \leqslant h \leqslant 12$; $-12 \leqslant k \leqslant 12$; $-7 \leqslant l \leqslant 7$), which correspond to 189 unique reflections, were measured and corrected for absorption, using Ψ-scans, and for Lorentz and polarization effects.

Magnetization measurements were performed on the as-cast and annealed polycrystalline samples, in zero-field cooling (ZFC) and field cooling (FC) studies. The measurements were carried out in the 2–300 K temperature range and under fields up to 7 T using a commercial SQUID MPMS-7 system (Quantum Design).

3. Experimental results and discussion

The weight losses during the preparation of the sample point to a small change in its nominal composition. Assuming that all the losses came from the evaporation of aluminium (the element with highest vapour pressure) a final $NpFe_4Al_{7.9}$ composition is obtained, very close to the ideal 1:4:8 elemental ratio.

No differences were observed between the powder x-ray diffraction data collected from annealed and as-cast samples, indicating a negligible influence of the heat treatment, which points to homogeneous samples and insignificant disorder effects in both materials. All the peaks of the diffraction patterns could be indexed according to the tetragonal $ThMn_{12}$-type structure (figure 1), the absence of extra peaks indicating a negligible, if any, concentration of impurity phases. The refinement of the lattice parameters gives $a = 8.7480(5)$ Å and $c = 5.0372(4)$ Å. The refined cell parameters and cell volume of $NpFe_4Al_8$ obtained from the x-ray powder diffraction measurements, together with those previously refined for the UFe_4Al_8 compound [6], are given in table 1.

The single-crystal x-ray diffraction data are compatible with a tetragonal system, space group $I4/mmm$. The structure was refined using the data for which $I > 3\sigma(I)$ (164

Table 1. The refined $NpFe_4Al_8$ lattice and cell volume, obtained from powder data, and positional parameters (x, y, z) from single-crystal data (the values for UFe_4Al_8 [6] are given within square brackets).

Lattice parameters (Å)					
a		8.7480(5)		[8.740(1)]	
c		5.0372(4)		[5.036(1)]	
Cell volume (Å^3)		385.48(8)		[384.7(2)]	
Atom	Position	*x*		*y*	*z*
Np [U]	2a	0		0	0
Fe	8f	1/4		1/4	1/4
Al	8j	0.2792(2)	[0.2805(2)]	1/2	0
Al	8i	0.3426(2)	[0.3440(2)]	0	0

unique observations), employing the program SHELXL-97 [19] and assuming a $ThMn_{12}$-type structure. The extinction factor, scale factor, two position parameters (x for the 8j and 8f positions) and twelve anisotropic temperature factors were all refined. The final refinement, down to $R = 0.018$, $R_W = 0.030$, confirms that in $NpFe_4Al_8$ the iron atoms are only at and completely fill the 8f positions. The aluminium atoms totally occupy the remaining 8j and 8i positions. The refined positional parameters obtained from the $NpFe_4Al_8$ single-crystal data, together with those previously refined for the UFe_4Al_8 compound [6], are listed in table 1.

From the comparison between the $NpFe_4Al_8$ and UFe_4Al_8 crystallographic data it can be seen that the neptunium compound has a unit cell volume slightly larger than the uranium one, due to both larger *a* and larger *c* cell parameters. This result is in apparent contradiction with the fact that the uranium metallic radius is greater than the neptunium radius (1.53 and 1.50 Å, for uranium and neptunium, respectively, considering a coordination number of 12 [20]). Previous studies on the UFe_4Al_8 compound indicated that there is a strong hybridization between the uranium 5f and the iron 3d states, which influences the cell parameters. Therefore, the larger cell parameters of the neptunium compound (when compared with UFe_4Al_8) are most probably due to a smaller (neptunium 5f)–(iron 3d) hybridization. This effect has been previously observed in other systems, for example, in the cubic $AnFe_2$ (An = actinide) Laves phase series: going from uranium to americium the compounds expand [21] as a result of the decrease in the hybridization (and, consequently, of the bonding), due to the contraction of the 5f orbital along the actinide series.

The number of nearest neighbours and interatomic distances (up to 3.5 Å), obtained from the single-crystal x-ray diffraction refinement for the different crystallographic positions, are listed in table 2. In $NpFe_4Al_8$, the minimum neptunium–neptunium distance is 5.0372 Å, well above the Hill critical limit (3.3 Å). The iron atoms are at 3.3395 Å from the neptunium, and the aluminium atoms range from 2.9971 to 3.174 Å, considerably above the sum of the metallic radii (2.76 and 2.93 Å for neptunium–iron and neptunium–aluminium, respectively, considering a metallic radius of 1.26 Å for iron and 1.43 Å for aluminium and a coordination number of 12 [20]). These high interatomic distances result in a weak hybridization between the neptunium 5f electrons and the 3d or 4s electrons of the iron atoms, and with the 3p electrons of the aluminium, that could result in an appreciable neptunium magnetic moment in $NpFe_4Al_8$.

Previous studies on RFe_4Al_8 (R = lanthanide, actinide, Y and La) have shown that the magnetic properties of this family of compounds are extremely sensitive to small changes in the iron concentration and disorder [17, 22, 23]. In the present case, the magnetization

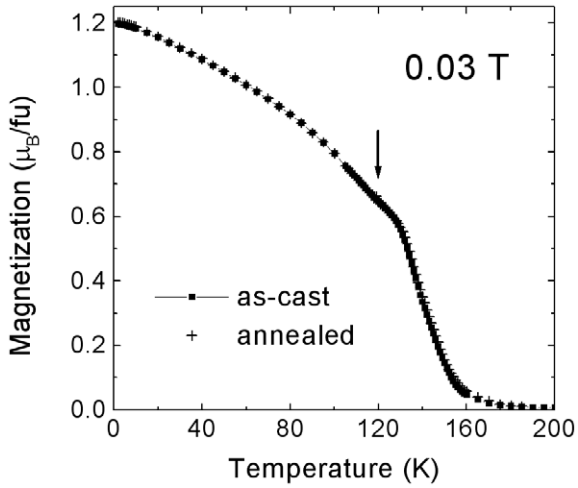

Figure 2. Magnetization as a function of temperature for the as-cast (squares) and annealed (crosses) $NpFe_4Al_8$ samples, in a field of 0.03 T.

Table 2. $NpFe_4Al_8$ interatomic distances (d) and nearest neighbour (NN) average numbers.

	NN	Atoms	d (Å)		NN	Atoms	d (Å)
Np (2a)	4	Al (8i)	2.9971(2)	Fe (8f)	2	Fe (8f)	2.5186(1)
	8	Al (8j)	3.1740(1)		4	Al (8j)	2.5366(3)
	8	Fe (8f)	3.3395(1)		4	Al (8i)	2.6505(4)
					2	Np (2a)	3.3395(1)
	1	Np (2a)	2.9971(2)				
Al (8j)	4	Fe (8f)	2.5366(3)	Al (8i)	4	Fe (8f)	2.6505(4)
	2	Al (8j)	2.7316(2)		2	Al (8j)	2.7347(1)
	2	Al (8i)	2.7347(1)		1	Al (8i)	2.7539(5)
	2	Al (8i)	2.8038(2)		2	Al (8j)	2.8038(2)
	2	Np (2a)	3.1740(1)		1	Np (2a)	2.9971(2)
					4	Al (8i)	3.1836(2)

measurements performed on the as-cast and on the annealed samples are identical, even for small applied fields, with exactly the same trends and signal magnitude, as shown in figure 2. This similarity between the magnetic behaviour of the as-cast and annealed samples points towards the same site occupation (composition and disorder) in the two samples, and indicates the absence of significant disorder, in agreement with the x-ray diffraction data.

The temperature dependence of the magnetization of the $NpFe_4Al_8$ as-cast sample, measured under different magnetic fields, upon warming after zero-field cooling and field cooling, is shown in figure 3. A ferromagnetic-type transition can be seen, which develops at $T_C = 135(2)$ K. This behaviour is similar to that observed for isostructural UFe_4Al_8, the $NpFe_4Al_8$ transition temperature being only slightly lower than in its uranium counterpart. In low field measurements, a small anomaly can be detected at 118(3) K, as can be seen in figure 2 for both the as-cast and the annealed samples. As no secondary phases could be detected from the x-ray powder pattern analysis, this anomaly is probably related to a reorientation of the iron moments or with the magnetic ordering of the neptunium atoms, decoupled from the iron sublattice, as suggested for previous $NpFe_4Al_{6.4}$ results [15].

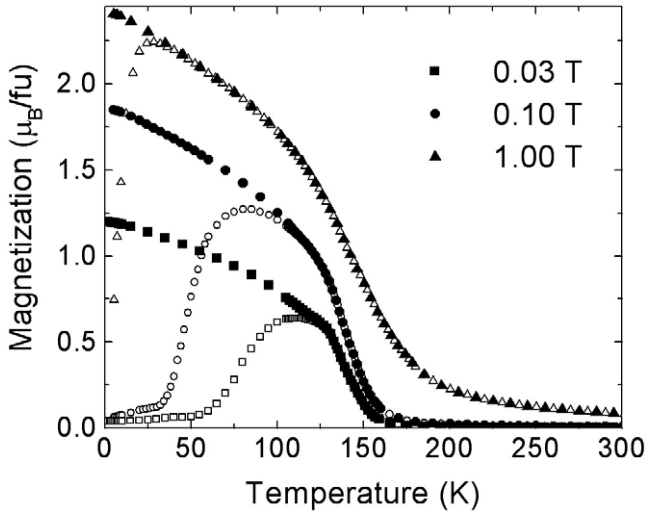

Figure 3. The temperature dependence of the magnetization of the $NpFe_4Al_8$ as-cast sample under various magnetic fields (full symbols: field cooled; open symbols: zero-field cooled).

For temperatures above 240 K the susceptibility follows a Curie–Weiss law, with an effective moment $\mu_{\text{eff}} = 7.9(1)\ \mu_B$ and a paramagnetic Curie temperature $\theta_P = 133(1)$ K. This effective moment is consistent with neptunium free ion configurations between Np^{3+} and Np^{5+} (μ_{eff} (Np) ranging from 2.75 to 3.68 μ_B [24]), implying a μ_{eff}(Fe) = 1.06–1.29 μ_B for $NpFe_4Al_8$ consistent with the 1.08(2) μ_B/Fe for UFe_4Al_8 obtained from single-crystal neutron diffraction data [6]. The paramagnetic Curie temperature is very close to the observed T_C, pointing to the existence of strong ferromagnetic interactions in $NpFe_4Al_8$.

The dependence of the magnetization, at different temperatures, with applied fields up to 7 T, is shown in figure 4. For temperatures below T_C the curves display a ferromagnetic-type behaviour, the extrapolated spontaneous magnetization for $T = 0$ K yielding $\mu_{\text{spont}} = 2.3\ \mu_B$/fu. This value is much smaller than the paramagnetic effective moment, indicating that $NpFe_4Al_8$ is not a simple ferromagnet.

It is also worth noting that the $NpFe_4Al_8$ spontaneous magnetization obtained is higher than the value found from UFe_4Al_8 magnetization measurements on single crystals (1.6 μ_B/fu) with the field parallel to the *a* easy axis. Assuming that the magnetic structure for $NpFe_4Al_8$ would be similar to the one obtained for the isostructural uranium compound, one may conclude that there is a higher iron ferromagnetic contribution and/or a large neptunium moment.

The resemblance between $NpFe_4Al_8$ and UFe_4Al_8 led us to perform a full magnetization cycle at 2 K (figure 5). This curve is characterized by a hysteresis with a step observed for fields between 1.3 and 1.75 T, reminiscent of that previously observed for UFe_4Al_8 single crystal [9]. This step can be allocated to a blocking of the ferromagnetic moments perpendicular to the external field, that occurs during the process of rotation of the domains towards the direction of B_{ext} [7]. The similarity between the physical properties of neptunium and uranium compounds, and successful experience with UFe_4Al_8 [3] and $UFe_{4+x}Al_{8-x}$ [25, 26], led us to perform band structure calculations on $NpFe_4Al_8$ in order to clarify the magnetic behaviour and calculate the magnetic structure of this compound.

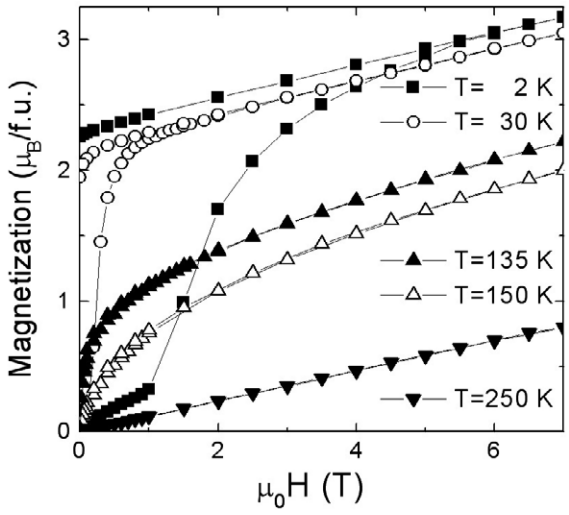

Figure 4. Magnetization curves of $NpFe_4Al_8$ as a function of magnetic field at various temperatures.

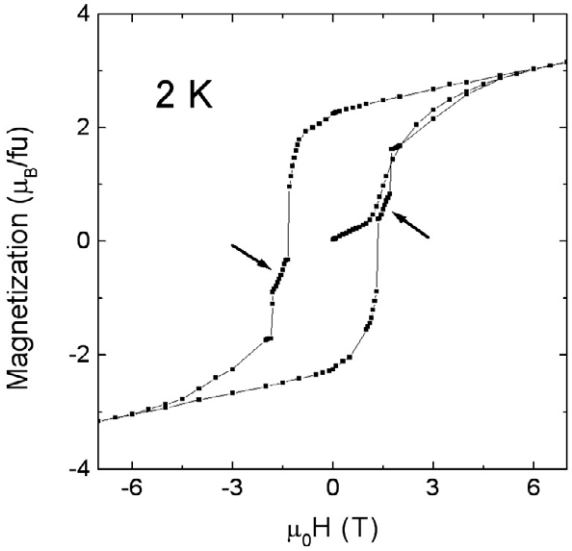

Figure 5. Virgin magnetization and magnetization cycles for $NpFe_4Al_8$ at 2 K.

4. Theoretical analysis

The calculations were performed using the augmented spherical waves (ASW) method modified to account for the noncollinear magnetic structure and relativistic interactions as described in [27–29]. 216 reciprocal lattice points were used in the irreducible part of the Brillouin zone. Convergence was confirmed by some calculations using 1000 k-points, where the moments varied by less than 0.02 μ_B/atom, the angles by less than 1° and the total energy by less than 0.5 mRyd/fu.

Table 3. Symmetry properties of the compound for several magnetic configurations. In the second column the number of Fe atoms refers to figure 7.

Operation	Permutation of Fe atoms				m_{spin} transformed from $(+m_x, +m_y, +m_z)$ to:
		Along *a*-or *b*-axis with SOC			
C_{2x} R	$1 \to 4$	$2 \to 3$	$3 \to 2$	$4 \to 1$	$(-m_x, +m_y, +m_z)$
I	$1 \to 1$	$2 \to 2$	$3 \to 3$	$4 \to 4$	$(+m_x, +m_y, +m_z)$
C_{2y}	$1 \to 3$	$2 \to 4$	$3 \to 1$	$4 \to 2$	$(-mx, +my, -mz)$
		Along *a*-or *b*-axis without SOC			
C_{2x}	$1 \to 4$	$2 \to 3$	$3 \to 4$	$4 \to 1$	$(+m_x, -m_y, -m_z)$
C_{2y}	$1 \to 3$	$2 \to 4$	$3 \to 1$	$4 \to 2$	$(-m_x, +m_y, -m_z)$
C_{2b}	$1 \to 1$	$2 \to 2$	$3 \to 4$	$4 \to 3$	$(-m_y, -m_x, -m_z)$
I	$1 \to 1$	$2 \to 2$	$3 \to 3$	$4 \to 4$	$(+m_x, +m_y, +m_z)$
		Along *c*			
C_{2x} R	$1 \to 4$	$2 \to 3$	$3 \to 4$	$4 \to 1$	$(-m_x, +m_y, +m_z)$
C_{2y} R	$1 \to 3$	$2 \to 4$	$3 \to 1$	$4 \to 2$	$(+m_x, -m_y, +m_z)$
C_{2b} R	$1 \to 1$	$2 \to 2$	$3 \to 4$	$4 \to 3$	$(+m_y, +m_x, +m_z)$
C_{4z-}	$1 \to 3$	$2 \to 4$	$3 \to 2$	$4 \to 1$	$(+m_y, -m_x, +m_z)$
C_{4z+}	$1 \to 4$	$2 \to 3$	$3 \to 1$	$4 \to 2$	$(-m_y, +m_x, +m_z)$
I	$1 \to 1$	$2 \to 2$	$3 \to 3$	$4 \to 4$	$(+m_x, +m_y, +m_z)$

4.1. Symmetry

The symmetry of the compound is the same as that of UFe_4Al_8 [3] and all of the comments made previously about the uranium compound's symmetry apply equally to $NpFe_4Al_8$; specifically, starting from a ferromagnetic structure with all the moments along the *c*-axis, the presence of a component of the iron magnetic moment along the *a*–*b* plane is possible without decreasing the symmetry of the structure. Alternatively, considering a ferromagnetic structure but now along one of the basal plane axes, one observes a similar effect: there is no decrease of symmetry if the iron moments have an antiferromagnetic projection perpendicular to the initial direction. In both of these cases any rotation of the neptunium moment implies a reduction of the symmetry of the crystal, and therefore the direction of the neptunium moments does not change. Thus the criterion for magnetic instability as used in [3] leads to a prediction of a collinear neptunium sublattice and a noncollinear structure for the iron sublattice for both of the above cases. The actual symmetry operations for the two magnetic structures, including spin–orbit coupling, are presented in table 3: the two cases (*a*–*b* plane and *c*-axis) have different symmetry operations.

One should note here that for this analysis it is essential to include relativistic effects, specifically spin–orbit coupling (SOC). The presence of SOC decreases the symmetry of the compound in a way that allows the iron moments to deviate from the collinear structure; symmetry analysis without SOC indicates that both the neptunium and iron moments can be ferromagnetically aligned, as is confirmed in one of the calculations presented in the next section.

The symmetry analysis is not able to predict the exact canting angles, nor can it indicate which of the proposed structures (canting from the *a*–*b* plane or canting from the *c*-axis) is actually the correct ground state structure. This must be determined by the full band structure calculations.

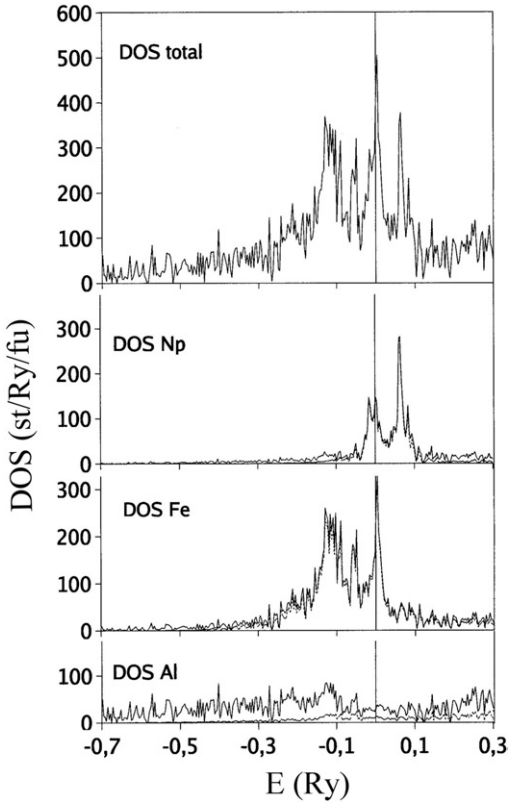

Figure 6. Densities of states for the nonmagnetic state of $NpFe_4Al_8$: (a) the total density of states, (b) the Np total (full curve) and 5f (broken curve) density of states, (c) the Fe total (full) and 3d (broken) density of states, (d) the Al total (full) and 3d (broken) density of states.

4.2. Nonmagnetic calculation and density of states

Figure 6 shows the calculated density of states (DOS) for a nonmagnetic state including spin–orbit coupling.

The neptunium atoms show two series of peaks. The first series, near the Fermi level, has two peaks very similar in both shape and magnitude. One of the peaks has its maximum exactly at E_{Fermi} and the other is about 18 mRyd below. The neptunium DOS at the Fermi level is 150 st/Ryd/atom. The second series of peaks is about 62 mRyd above the E_{Fermi} and have twice the magnitude of the peaks just mentioned, DOS $=$ 285 st/Ryd/atom. The distance between the two is about 68 mRyd which gives a rough estimate of the magnitude of the SOC splitting.

Below E_{Fermi} the 3d states give the main contribution to the total DOS. 0.1 Ryd below the Fermi level there is a broad series of 3d peaks with an average height of 60 states Ryd^{-1}/atom. Between this series and the Fermi level there are two slightly smaller peaks.

In figure 6 it can be seen that both the 3d and the 5f states contribute significantly to the DOS at the E_{Fermi}.

4.3. Magnetic structure

Spin polarized calculations were performed for several magnetic structures and all show a total energy (E_{total}) lower than the nonmagnetic state, confirming the instability of the nonmagnetic

Table 4. Calculated magnetic moments of several magnetic structures. θ is the angle between the magnetic moment of each atom and the **c**-axis; ϕ is the angle between the projection in the **a**–**b** plane of the magnetic moment and the a-axis; m_{spin}, m_{orb} and m_{total} are the spin orbital and total moment for each atom in μ_B; M is the total moment of a formula unit, including the Al contribution. ΔE is the difference between the total energy of the configuration and that of our ground state, in mRyd/fu. In the first two calculations the moments (a) were constrained to be nonmagnetic. In the third calculation the directions (b) were fixed. In the last two calculations both values and directions were calculated self-consistently.

Atom	θ	ϕ	m_{spin}	m_{orb}	m_{total}
		Np nonmag.			
Np	NM[a]				
Fe	90°	8°	1.34	0.08	1.42
	$M = 5.62\ \mu_B$/fu			$\Delta E = 10$	
		Fe nonmag.			
Np	90°	90°	3.21	−3.30	−0.09
Fe	NM[a]				
	$M = 0.09\ \mu_B$/fu			$\Delta E = 18$	
		Imposed ferromag. (along b-axis)			
Np	90° (b)	90° (b)	3.02	−3.36	−0.34
Fe	90° (b)	90° (b)	1.29	0.07	1.36
	$M = 4.78\ \mu_B$/fu			$\Delta E = 4$	
		Free rotation: initially along c-axis			
Np	0°	0°	3.01	−3.42	−0.41
Fe	2°	45°	1.27	0.08	1.35
	$M = 4.66\ \mu_B$/fu			$\Delta E = 4$	
		Free rotation: initially in a–b plane			
Np	90°	90°	3.33	−3.20	0.13
Fe	90.6°	257°	1.37	0.07	1.44
	$M = 5.07\ \mu_B$/fu			$\Delta E = 0$	

state. Prediction of the actual ground state structure is made via a comparison of E_{total} for the different magnetic structures. The results are summarized in table 4.

Since the magnetic structure is complex, and in order to study the interdependence of the iron and neptunium moments, various calculations were performed, allowing for noncollinear magnetic structures. Constraining the iron lattice to be nonmagnetic, neptunium develops appreciable spin and orbital moments, although due to their antiparallel coupling the total moment is small. Thus the presence of a neptunium moment does not depend upon the presence of the iron moments; this situation is different from that for the UFe_4Al_8 compound, where the uranium moment is induced by the iron moments. Similarly to the UFe_4Al_8 case, the imposition of a zero moment on the actinide atom does not inhibit the formation of moments on the iron atoms. The iron moments are now almost perpendicular to the direction previously defined by the neptunium moment, with a canting angle of 82°.

Comparing collinear ferromagnetic structures with all the moments along the c-or the b-axes, the calculations confirm the general result of the symmetry analysis: neither of these magnetic structures is stable; when the moments are left free to rotate the iron moments deviate from the initial alignment. The neptunium moments, although left free to rotate in the calculation, do not rotate.

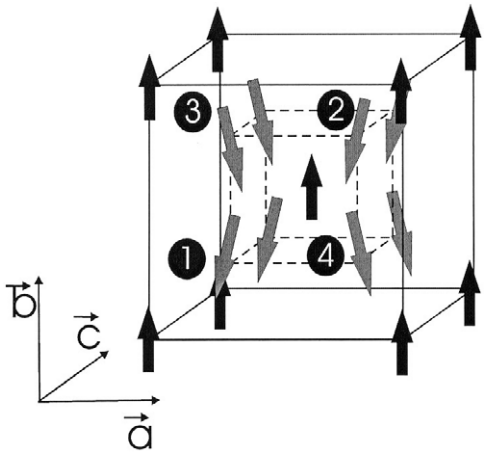

Figure 7. Calculated ground state magnetic structure. The arrows indicate the spin orientation of the Np (black) and Fe (grey) atoms. The Fe atoms are numbered 1–4 in accordance with table 3, which presents the interchange of the Fe atoms under the various symmetry operations.

Starting a calculation with the moments along the *c*-axis, the iron moments deviate by 1.8° from the *c*-axis. The projection on the *a*–*b* plane is antiferromagnetic.

Starting a calculation with the moments aligned along one of the axes of the *a*–*b* plane, the iron moments assume a noncollinear antiferromagnetic structure that deviates about 13° from the neptunium moments with an antiferromagnetic component perpendicular to the initial direction. The neptunium maintains the initial direction. This magnetic structure has an E_{total} 4 mRyd lower than the structure that results from the state starting with all the moments along the *c*-axis, and is illustrated in figure 7.

Comparing the values for the calculated moments, we see that the spin and orbital moments do not vary greatly with alterations in the conditions; that is, that the atomic moments do not depend strongly upon the relative orientation of the atomic moments. The neptunium spin and orbital moments have similar values and, since they are antiparallel, the neptunium total moment is small.

Summarizing, according to the calculations, the last structure described above is the strongest candidate for being the ground state structure. It is similar to the structure of the UFe_4Al_8 compound: all the moments are in the *a*–*b* plane; the neptunium sublattice has a ferromagnetic structure along one of the basal plane axes; the iron lattice is canted by 13° relatively to the neptunium moments with an antiferromagnetic projection perpendicular to these moments. This value should be compared with the 74° angle between the uranium and iron moments in UFe_4Al_8, where both elements contribute to the ferromagnetic component. In the neptunium analogue the magnetic coupling may be reversed, depending on the magnitude of the spin and orbital contributions of the neptunium atom.

4.4. Variation of spin–orbit coupling and orbital polarization correction

In order to test the sensitivity of our results to the exact treatment of the spin–orbit coupling (SOC), various calculations were performed, enhancing the magnitude of the coupling by a linear scaling factor. The first result presented in table 5 is for a calculation without the inclusion of SOC. After convergence, both moments, neptunium and iron, are still aligned along the same axis, one of the basal plane axes. With the inclusion of SOC and subsequent

Table 5. The magnitude and direction of moments calculated self-consistently for different spin–orbit coupling (SOC) magnitudes and the application of the orbital polarization correction (OPC): the SOC term in the Hamiltonian is multiplied by a linear scaling factor (the usual calculation corresponds to a scaling factor of 1), in the table referred to as the 'SOC scale'. Orbital polarization is applied as $H_{\mathrm{OP}}C = I_{\mathrm{OPC}}Lm_l$. θ is the angle between the magnetic moment of each atom and the **c**-axis; ϕ is the angle between the projection in the **a**–**b** plane of the magnetic moment and the a-axis; m_{spin}, m_{orb} and m_{total} are the spin orbital and total moment for each atom in μ_{B}; M is the total moment of a formula unit, including the Al contribution. ΔE is the difference between the total energy of the configuration and that of our ground state, in mRyd/fu.

Atom	θ	ϕ	m_{spin}	m_{orb}	m_{total}
	SOC = 0		$I_{\mathrm{OPC}} = 0$		
Np	90°	90°	3.40	—	3.40
Fe	90°	90°	1.26	—	1.26
	$M = 8.19\ \mu_{\mathrm{B}}$/fu		$E_{\mathrm{total}} = +38$		
	SOC = 1		$I_{\mathrm{OPC}} = 0$		
Np	90°	90°	3.33	−3.20	0.13
Fe	90.6°	257°	1.37	0.07	1.44
	$M = 5.07\ \mu_{\mathrm{B}}$/fu		$E_{\mathrm{total}} = 0$		
	SOC = 1.1		$I_{\mathrm{OPC}} = 0$		
Np	90°	90°	3.25	−3.29	−0.04
Fe	90.6°	257°	1.36	0.07	1.43
	$M = 5.21\ \mu_{\mathrm{B}}$/fu		$E_{\mathrm{total}} = -5$		
	SOC = 1.4		$I_{\mathrm{OPC}} = 0$		
Np	90°	90°	2.87	−3.30	−0.43
Fe	90.6°	257°	1.34	0.09	1.44
	$M = 5.78\ \mu_{\mathrm{B}}$/fu		$E_{\mathrm{total}} = -29$		
	SOC = 1		$I_{\mathrm{OPC}} = 1$ mRyd		
Np	90°	90°	3.39	−3.78	−0.39
Fe	90.6°	258°	1.36	0.07	1.44
	$M = 5.61\ \mu_{\mathrm{B}}$/fu		$E_{\mathrm{total}} = -1$		
	SOC = 1		$I_{\mathrm{OPC}} = 2$ mRyd		
Np	90°	90°	3.46	−4.26	−0.80
Fe	90.7°	261°	1.36	0.07	1.43
	$M = 6.03\ \mu_{\mathrm{B}}$/fu		$E_{\mathrm{total}} = -7$		

lowering of the compound's symmetry, the iron moments rotate (freely) to the values given in table 5. The change in SOC scale obviously does not alter the symmetry of the compounds and for all calculations (except for SOC = 0) the same magnetic structure is found, differing only in terms of the exact canting angle. The values of the iron moments are insensitive to the changes in SOC scale; the neptunium orbital moment increases and the neptunium spin moment decreases slightly. As the two quantities are coupled antiferromagnetically, the total moment of neptunium changes sign; however, the neptunium moment is always found to be less than 0.5 μ_{B}/fu.

Furthermore, in order to increase the m_l splitting, modelling Hund's second rule in this way, we add to the Hamiltonian an orbital polarization correction (OPC) of the form $H_{\mathrm{OPC}} = I_{\mathrm{OPC}}Lm_l$, as applied in [3]. The normal effect of this term is increase of the orbital moment of the actinides, although for UFe_4Al_8 this simple term had a complex effect [3]. The

first result presented in table 5 is for a calculation without SOC—the moments are aligned along the same axis. With the inclusion of SOC and subsequent lowering of the compound's symmetry, the iron moments rotate (freely) to the values given in table 5. As noted in the previous section, the neptunium moments, although left free to rotate in the calculation, do not rotate. This is of course obvious, as the nonrotation of the neptunium atoms is linked to the symmetry of the compound, which does not suffer any alteration with the variation of the SOC parameter or the inclusion of OPC. The iron canting angle is relatively indifferent to the SOC parameter and to the introduction of the OPC. The main effect of both SOC and OPC is, as one would expect, to increase the neptunium orbital moment.

5. Conclusions

The structural results presented in this work for a stoichiometric $NpFe_4Al_8$ sample confirm that it crystallizes in the $ThMn_{12}$-type structure, with the iron atoms only occupying the 8f crystallographic sites. The results for the lattice and internal parameters are consistent with those for other stoichiometric compounds of the $AnFe_4Al_8$ series and point to a smaller neptunium 5f–iron 3d hybridization when compared with the isostructural uranium compound.

Magnetization measurements indicate that the magnetic properties of the $NpFe_4Al_8$ compound are similar to those of UFe_4Al_8. Independently, symmetry analysis shows that the neptunium atoms should form a collinear magnetic structure, with a noncollinear magnetic structure for the iron atoms. First-principles calculations yield a ground state magnetic structure similar to that of UFe_4Al_8, and completely compatible with the experimental observations. Thus, on the basis of the combined results of the magnetization measurements, symmetry analysis and full calculations, we conclude that the magnetic structure of $NpFe_4Al_8$ is well described as a lattice of neptunium ferromagnetically aligned along the *b*-axis, with the iron atoms forming a noncollinear structure in the *a*–*b* plane (figure 7). This is basically identical to the UFe_4Al_8 magnetic structure, but with a higher canting angle of the iron magnetic moments, which puts them almost antiparallel to the neptunium moments, at variance with the uranium analogue, where the iron moments have a smaller canting. Magnetization versus temperature measurements show an ordering temperature of $T_C = 135(2)$ K, with a second anomaly at 118(3) K. Previous neptunium Mössbauer spectroscopy measurements on a nonstoichiometric $NpFe_4Al_{6.4}$ sample indicate that the two magnetic sublattices, neptunium and iron, could order at different temperatures [15]. Our calculations show that, unlike the case for the sister UFe_4Al_8 compound, in the stoichiometric $NpFe_4Al_8$ compound the two magnetic sublattices order independently, as suggested by the two anomalies observed in the magnetization measurements. It is also to be noted that the difference between the calculated total moment per formula unit (5–6 μ_B) and the $T = 0$ K extrapolated spontaneous magnetization obtained from the polycrystalline data ($\mu_{spont} = 2.3\ \mu_B$/fu) could be explained by the compound's magnetic anisotropy, similar to that observed in UFe_4Al_8.

Acknowledgments

The high purity neptunium metal required for this work was made available through a loan agreement between Lawrence Livermore National Laboratory and ITU, in the framework of a collaboration involving LLNL, Los Alamos National Laboratory and the US Department of Energy. A P Gonçalves acknowledges financial support for access to the Actinide User Laboratory at ITU-Karlsruhe within the framework of the European Community Access to Research Infrastructures action of the Improving Human Potential Programme (IHP), contract

HPRI–CT-2001–00118. Part of the work was supported by the FCT/POCTI/35338/FIS/2000 co-funded by the European Community FEDER.

References

[1] Recko K, Szymanski K, Dobrzynski L, Satula D, Suski W, Wochowski K, Andre G, Bouree F and Hoser A 2002 *J. Alloys Compounds* **334** 58
[2] Marques J G, Barradas N P, Alves E, Ramos A R, Gonçalves A P, da Silva M F and Soares J C 2001 *Hyperfine Interact.* **136** 333
[3] Sandratskii L M and Kübler J 1999 *Phys. Rev.* B **60** R6961
[4] Szymanski K, Recko K, Dobrzynski L and Satula D 1999 *J. Phys.: Condens. Matter* **11** 6451
[5] Waerenborgh J C, Gonçalves A P, Bonfait G, Godinho M and Almeida M 1999 *Phys. Rev.* B **60** 4074
[6] Paixão J A, Lebech B, Gonçalves A P, Brown P J, Lander G H, Burlet P, Delapalme A and Spirlet J C 1997 *Phys. Rev.* B **55** 14370
[7] Bonfait G, Godinho M, Estrela P, Gonçalves A P, Almeida M and Spirlet J C 1996 *Phys. Rev.* B **53** R480
[8] Bonfait G, Gonçalves A P, Spirlet J C and Almeida M 1995 *Physica* B **211** 139
[9] Godinho M, Bonfait G, Gonçalves A P, Almeida M and Spirlet J C 1995 *J. Magn. Magn. Mater.* **140** 1417
[10] Andreev A V, Nakotte H and DeBoer F R 1992 *J. Alloys Compounds* **182** 55
[11] Stepien-Damm J, Baran A and Suski W 1984 *J. Less-Common Met.* **102** L5
[12] Li H-S and Coey J M D 1991 *Handbook of Magnetic Materials* vol 6, ed K H J Buschow (Amsterdam: Elsevier Science) p 1
[13] Gal J, Pinto H, Fredo D, Shaked H, Schäfer W, Will G, Litterst F J, Potzel W, Asch L and Kalvius G M 1987 *Hyperfine Interact.* **33** 173
[14] Schäfer W, Will G, Gal J and Suski W 1989 *J. Less-Common Met.* **149** 237
[15] Gal J, Yaar I, Regev D, Fredo S, Shani G, Arbaboff E, Potzel W, Aggarwal K, Pereda J A, Kalvius G M, Litterst F J, Schäfer W and Will G 1990 *Phys. Rev.* B **42** 8507
[16] Schäfer W, Will G and Gal J 1991 *Eur. J. Solid State Inorg. Chem.* S **28** 563
[17] Kuznietz M, Gonçalves A P, Waerenborgh J C, Almeida M, Cardoso C, Cruz M-M and Godinho M 1999 *Phys. Rev.* B **60** 9494
[18] Rodriguez-Carvajal J 1993 *Physica* B **192** 55
[19] Sheldrick G M 1997 *SHELX-97-Program for Crystal Structure Solution and Refinement* University of Göttingen, Germany
[20] Vainshtein B K, Fridkin V M and Indenbom V L 1982 *Springer Series in Solid-State Sciences* vol 21, ed M Cardona, P Fulde and H-J Queisser (Berlin: Springer) p 71
[21] Sechovsky V and Havela L 1988 *Ferromagnetic Materials* vol 4, ed E P Wohlfarth and K H J Buschow (Amsterdam: Elsevier Science) p 309
[22] Waerenborgh J C, Salamakha P, Sologub O, Gonçalves A P, Sério S, Godinho M and Almeida M 2001 *J. Alloys Compounds* **317/318** 44
[23] Waerenborgh J C, Salamakha P, Sologub O, Gonçalves A P, Cardoso C, Sério S, Godinho M and Almeida M 2000 *Chem. Mater.* **12** 1743
[24] Fournier J-M and Troc R 1985 *Handbook on the Physics and Chemistry of the Actinides* vol 2, ed A J Freemann and G H Lander (Amsterdam: North-Holland) p 29
[25] Cardoso C, Sandratskii L M, Gasche T and Godinho M 2002 *Phys. Rev.* B **65** 94413
[26] Cardoso C, Sandratskii L M, Gasche T and Godinho M 2003 *Phys. Status Solidi* **326** 544
[27] Sandratskii L M 1998 *Adv. Phys.* **47** 91
[28] Sandratskii L M, Kübler J, Zahn P and Mertig I 1994 *Phys. Rev.* B **50** 21
[29] Sticht J, Höck K-H and Kübler J 1989 *J. Phys.: Condens. Matter* **1** 8155